Rich CNN-Transformer Feature Aggregation Networks for Super-Resolution

1

Jinsu Yoo*†, Taehoon kim[‡], Sihaeng Lee[‡], Seung Hwan Kim[‡], Honglak Lee[‡], and Tae Hyun Kim*§

*Hanyang University, Seoul, South Korea

[‡]LG AI Research, Seoul, South Korea

Abstract

Recent vision transformers along with self-attention have achieved promising results on various computer vision tasks. In particular, a pure transformer-based image restoration architecture surpasses the existing CNN-based methods using multi-task pre-training with a large number of trainable parameters. In this paper, we introduce an effective hybrid architecture for super-resolution (SR) tasks, which leverages local features from CNNs and long-range dependencies captured by transformers to further improve the SR results. Specifically, our architecture comprises of transformer and convolution branches, and we substantially elevate the performance by mutually fusing two branches to complement each representation. Furthermore, we propose a cross-scale token attention module, which allows the transformer to efficiently exploit the informative relationships among tokens across different scales. Our proposed method achieves state-of-the-art SR results on numerous benchmark datasets.

I. Introduction

Super-resolution (SR) is a longstanding problem that aims to restore a high-resolution (HR) image from the given low-resolution (LR) image. Early researchers attempted to mitigate the ill-posed nature of the SR task by minimizing energy models with multiple priors and likelihood models [17, 18, 52, 60].

With the advancements in deep learning, various CNN-based SR methods are introduced [10, 28, 30, 33, 40, 42, 57, 64], which utilize numerous approaches such as residual connection [28, 33], channel attention [42, 64], and non-local operation [34, 40, 65]. The emergence of CNN-based SR networks has verified the efficiency in processing 2D images with the inductive bias (*e.g.*, local connectivity and translation invariance). However, such architectures have certain limitations in capturing long-range dependencies [11] and restoring weak texture details [6].

The transformer [54] has recently gained special attention in the natural language processing (NLP) community thanks to its impressive performance. The key component that contributes to the success is a self-attention mechanism, which beneficially captures long-range dependencies among input sequences. Several researchers have also adopted the transformer to solve computer vision problems, and the vision transformer (ViT) [11] for the image classification task is a pioneering work. Since then, many follow-up studies have been introduced for various vision tasks, such as image classification [53,61], object detection [4,67], and dense prediction [44,62].

ViTs have several advantages over conventional CNNs. Particularly, self-attention operation free from the locally-connected constraint enables a network to learn long-range spatial dependencies within the input image, which also shows the applicability of transformer for the restoration tasks [3,6,32,58]; that is, the transformer architecture inherently contains superiority over CNN in exploiting self-similar patches [68] within the input image. Such a procedure is explicitly implemented in the self-attention mechanism as it calculates similarity among tokens (patches) over the entire input image.

However, simply applying conventional ViT [11] to the SR task raises several concerns. First, ViTs have been mainly validated on the high-level vision tasks (*e.g.*, image classification). Thus, the role of each component inside a transformer (*e.g.*, positional embeddings) for the low-level vision tasks, such as image restoration, remains to be studied. Second, the image restoration solely with the tokenized image patches can cause undesired artifacts at the token boundaries. Such a problem can be alleviated by tokenization with large overlapping, but this approach quadratically increases the computational cost for self-attention. Moreover, tokenization with an identical token size limits the exploitation of multi-scale features. Notably, reasoning across different scaled patches (tokens) are shown to be exceptionally beneficial in SR [23, 43, 50] as it utilizes the internal self-similar patches [68].

In this paper, we first introduce an effective hybrid architecture that takes advantage of CNN and recent ViT. Specifically, we propose two different branches (*i.e.*, CNN and transformer branches), and aggregate them several

Preprint.

Work done during an internship at LG AI Research.

[§] Corresponding author.

times during the SR procedure. Consequently, local features extracted from the CNN branch and long-range dependencies captured in the transformer branch are progressively fused to complement each other and extract rich features. Furthermore, we propose a cross-scale token attention module, which overcomes the limitation of conventional ViTs [6, 11] in exploiting multi-scale features, and substantially improves the SR performance. Moreover, we investigate the necessity of commonly used techniques with transformers, such as positional embeddings, for SR tasks rather than the high-level vision tasks.

The proposed method which aggregates both CNN and transformer features, namely ACT, achieves new state-of-the-art SR performances on numerous benchmark datasets and even remarkably outperforms recent transformer-based methods [6, 32]. In summary, our contributions are presented as follows:

- We introduce a novel hybridized SR method, namely ACT, which combines CNN and ViT.
- We propose the cross-scale token attention module to leverage multi-scale token representations efficiently.
- We conduct extensive experiments and demonstrate the superiority of ACT on numerous benchmark SR datasets.

II. RELATED WORKS

In this section, we survey representative works on SR, ViTs, and multi-stream networks related to our work.

A. Image super-resolution

Starting from the seminal work by Dong *et al.* [10], numerous CNN-based SR networks have been introduced. Kim *et al.* [28] brought the residual connection [21] to construct deep networks, and Son *et al.* [33] further analyzed the residual block to suit for the SR task. Zhang *et al.* [64] built considerably deep networks with residual-in-residual structures and also proposed the channel attention block to enhance the feature representation. Incrementally, Niu *et al.* [42] introduced the layer attention module to gain extra information among layers. Moreover, Dai *et al.* [8] strengthened the network representation by introducing the second-order attention module, while Guo *et al.* [20] introduced the dual regression network with the closed-loop constraint.

Meanwhile, researchers also have focused on exploiting non-locality within an image [68]. Among them, Liu et al. [34] incorporated the non-local operation with deep recurrent neural network (RNNs), whereas Zhang et al. [65] allowed the non-local block to guide the local block by passing additional information. To exploit recurring patches across scales, Mei et al. [41] introduced the RNN-based cross-scale non-local attention module, while Zhou et al. [66] utilized the graph neural networks. Recently, Mei et al. [40] introduced bucket-based sparse attention to reduce the computational complexity. Different from existing studies, we leverage ViT [11] to capture global representations. Moreover, our CNN branch is not restricted to any certain architecture.

B. Vision transformer (ViT)

Transformer [54] was initially introduced in the NLP community as a substitute to the recurrent scheme to boost its scalability. In computer vision, Dosovitskiy *et al.* [11] borrowed the transformer architecture for the first time, and proposed ViT to solve the image classification task by reshaping an image into flattened patches. Numerous tasks have employed ViT (*e.g.*, object detection [4,67], dense prediction [35,44], restoration [3,58]), whereas some researchers have investigated to bring locality to the transformer [12,19,31,35,56,59]. For image SR, Chen *et al.* [6] proposed a pure ViT-based network [11] to handle various image restoration tasks, including denoising, deraining, and SR. The network is pre-trained with multi-task manners, including the entire tasks, and fine-tuned to the desired task (*e.g.*, \times 2 SR). Instead of the standard self-attention, Liang *et al.* [32] adapted the Swin Transformer block [35] and included convolutional layers inside the block to impose the local connectivity. Our work is especially motivated to overcome the limitations within the IPT [6] such as the need for multi-task learning and lots of parameters, and lack of multi-scale representations.

Few works have studied leveraging multi-scale token representations. Among them, Chen *et al.* [5] explicitly tokenized an image with different token sizes, while Wang *et al.* [56] constructed the pyramid architecture. By contrast, we maintain a single token representation, while utilizing channel-wise splitting to generate multi-scale tokens in time and reasoning across them efficiently.

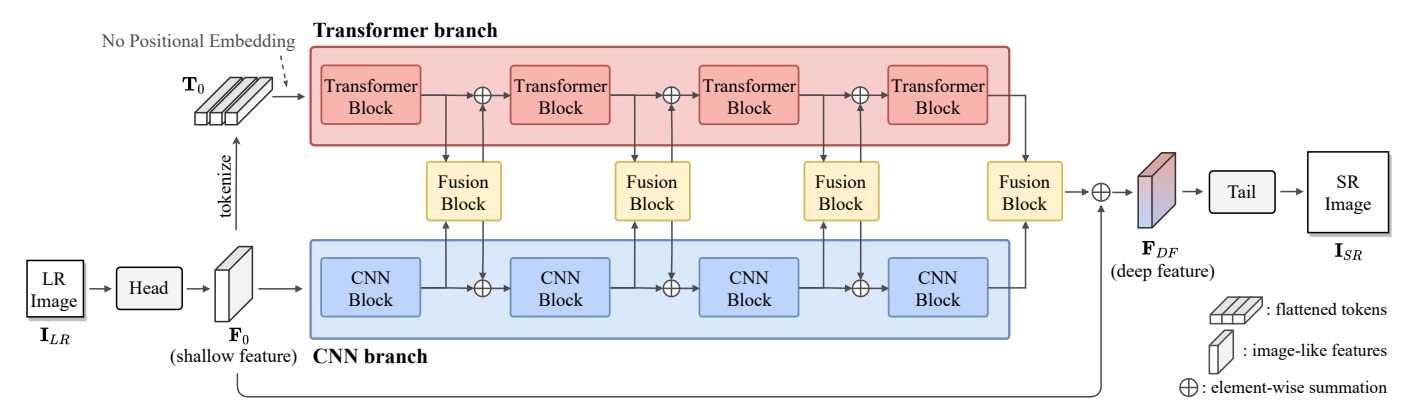


Fig. 1: Overall flow of ACT. The input image goes through two separate branches constructed with a CNN and ViT. Each branch extracts local features and global representations, and actively exchanges beneficial information during the intermediate fusion. Final SR result is acquired by aggregating both representations.

C. Multi-stream approaches

Multi-stream networks [7, 14–16, 51] have been proposed to effectively treat several input data containing different information. For SR, Jin *et al.* [27] and Isobe *et al.* [25] decomposed the input image/video into structural and texture information to advantageously enhance the missing high-frequency details. Different from these works, we borrow the recent ViT to enrich model capacity and global connectivity.

III. PROPOSED METHOD

In this section, we present the proposed ACT network which leverages CNN and transformer in detail. ACT is composed of a shallow feature extraction module (head), transformer/CNN modules (body), and a high-quality image reconstruction module (tail). The overall structure of ACT is given in Figure 1.

A. Head

First, the head module H_{Head} extracts shallow feature \mathbf{F}_0 from a given low-resolution input image \mathbf{I}_{LR} as:

$$\mathbf{F}_0 = H_{Head}(\mathbf{I}_{LR}),\tag{1}$$

where H_{Head} comprises of two residual convolution blocks as suggested in previous works [6, 33, 64].

B. Body

Next, the extracted feature \mathbf{F}_0 is passed to the body module to acquire rich features as:

$$\mathbf{F}_{DF} = H_{Body}(\mathbf{F}_0) + \mathbf{F}_0, \tag{2}$$

where \mathbf{F}_{DF} indicates deep feature, and H_{Body} contains the proposed two-stream branches to extract residual features correspondingly. Notably, the body module can solely focus on restoring the high-frequency details as the long skip connection directly passes the low-frequency information to the tail module (see "Feature visualization" in Section IV-B4).

1) CNN branch: In the body module, convolutional kernels in CNN branch slide over the image-like features with a stride of 1. Such a procedure compensates for the lack of intrinsic inductive bias in the transformer branch. In building our CNN branch, we adopt residual channel attention module (RCAB) [64], which has been widely used in the recent SR approaches [20, 42]. Specifically, we stack N CNN Blocks, which yields the following:

$$\mathbf{F}_i = H_{CB}^i(\mathbf{F}_{i-1}), \quad 1 \le i \le N, \tag{3}$$

where H_{CB}^i denotes the CNN Block including the RCAB modules, and \mathbf{F}_i represents the extracted CNN feature at the *i*th CNN Block.

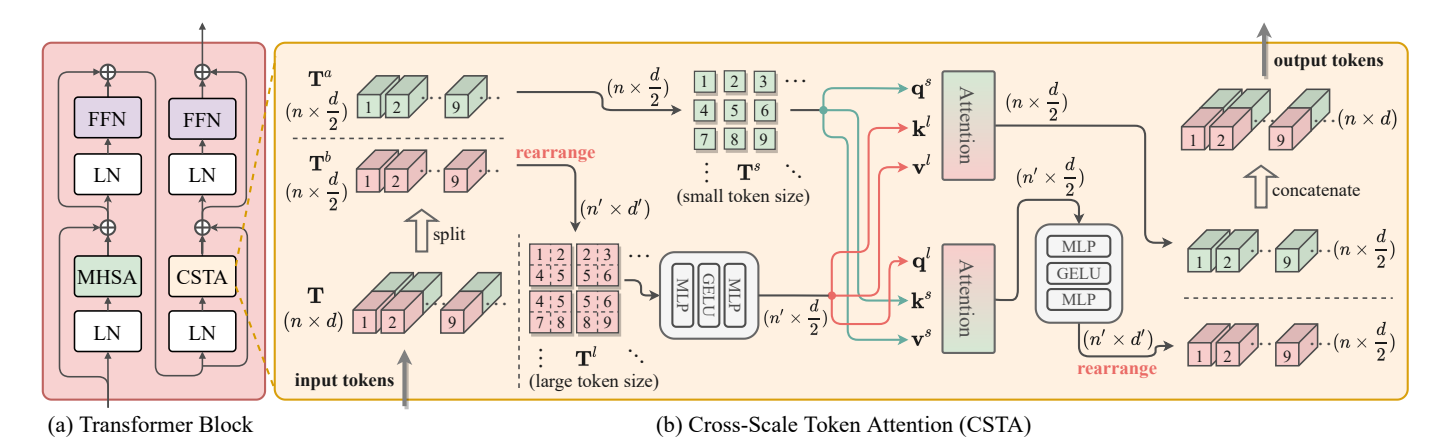


Fig. 2: (a) Our Transformer Block includes multi-head self-attention (MHSA) and cross-scale token attention (CSTA) to fully leverage informative feature representations on a multi-scale. (b) CSTA effectively exploits information across different scaled tokens by channel-wise splitting and token rearrangement. Two different token embeddings exchange keys and values for the attention.

2) Transformer branch: We construct a transformer branch in the body module based on the conventional multihead self-attention (MHSA) [6, 11]. Moreover, we propose to add cross-scale token attention (CSTA) modules in the transformer branch to exploit repeating structures within an input image across different scales.

First, we tokenize the image-like shallow feature $\mathbf{F}_0 \in \mathbb{R}^{c \times h \times w}$ into non-overlapping n tokens $\mathbf{T}_0 \in \mathbb{R}^{n \times d}$, where d means the dimension of each token vector. Notably, $n = h/t \times w/t$ and $d = c \cdot t^2$ when t is the token size. Moreover, unlike previous ViTs [6, 11], we observe that positional information becomes insignificant in SR. Thus, we do not add the positional embeddings to the tokens (see our ablation of "Impact of positional embeddings" in Section IV-B1).

The acquired tokens are then fed into transformer branch, including N number of Transformer Blocks, which is symmetric to CNN branch as:

$$\mathbf{T}_i = H_{TB}^i(\mathbf{T}_{i-1}), \quad 1 \le i \le N, \tag{4}$$

where T_i indicates the extracted token representations at the *i*th Transformer Block H_{TB}^i . As depicted in Figure 2 (a), each Transformer Block includes two sequential attention operations: multi-head self-attention (MHSA) [6, 11] and cross-scale token attention (CSTA), which yield:

$$\mathbf{T}''_{i-1} = FFN(LN(\mathbf{T}'_{i-1})) + \mathbf{T}'_{i-1}, \mathbf{T}'_{i-1} = MHSA(LN(\mathbf{T}_{i-1})) + \mathbf{T}_{i-1}$$

$$\mathbf{T}_{i} = FFN(LN(\mathbf{T}''_{i-1})) + \mathbf{T}''_{i-1}, \mathbf{T}''_{i-1} = CSTA(LN(\mathbf{T}''_{i-1})) + \mathbf{T}''_{i-1},$$
(5)

where FFN (feed forward network) includes two MLP layers with expansion ratio r with GELU activation function [22] in the middle of the layers, LN denotes the layer normalization [1], and the details of our CSTA are as follows.

Cross-scale token attention (CSTA): Standard MHSA [11,54] performs attention operation by projecting queries, keys, and values from the same source of single-scale tokens. In addition to the self-attention, we propose to exploit the information from tokens across different scales, and we illustrate the operational flow of the proposed CSTA module in Figure 2 (b) and provide pseudocode in our Appendix for clarification. Concretely, we split input token embeddings $\mathbf{T} \in \mathbb{R}^{n \times d}$ of CSTA along the last (i.e., channel) axis into two, and we represent them as $\mathbf{T}^a \in \mathbb{R}^{n \times d/2}$ and $\mathbf{T}^b \in \mathbb{R}^{n \times d/2}$. Then, we generate $\mathbf{T}^s \in \mathbb{R}^{n \times d/2}$ and $\mathbf{T}^l \in \mathbb{R}^{n' \times d'}$, which include n tokens from \mathbf{T}^a and n' tokens by simply rearranging \mathbf{T}^b , respectively. In practice, we use \mathbf{T}^a for \mathbf{T}^s as is, and re-tokenize [61] \mathbf{T}^b to generate \mathbf{T}^l with larger token size and overlapping. Here, we can control the number of tokens in \mathbf{T}^l by setting as $n' = \lfloor \frac{h-t'}{s'} + 1 \rfloor \times \lfloor \frac{w-t'}{s'} + 1 \rfloor$, where s' is the stride and t' denotes the token size, and the token dimension is $d' = (c/2) \cdot t'^2 = (d \cdot t'^2)/2t^2$. One can acquire numerous tokens of large size by overlapping, which enables the network to actively enjoy patch-recurrence across scales. We note that large tokens serve as an important pool for reasoning repeating patches across scales during the CSTA procedure.

In particular, to effectively improve the SR performance by exploiting self-similar patches across different scales and passing information from a larger patch to small but self-similar ones, we produce a smaller number of tokens

(i.e., n' < n) with a relatively larger token size (i.e., t' > t), and then compute cross-scale attention scores between tokens in both \mathbf{T}^s and \mathbf{T}^l .

Specifically, we generate queries, keys and values in \mathbf{T}^s and \mathbf{T}^l : $(\mathbf{q}^s \in \mathbb{R}^{n \times d/2}, \mathbf{k}^s \in \mathbb{R}^{n \times d/2}, \mathbf{v}^s \in \mathbb{R}^{n \times d/2})$ from \mathbf{T}^s , and $(\mathbf{q}^l \in \mathbb{R}^{n' \times d/2}, \mathbf{k}^l \in \mathbb{R}^{n' \times d/2}, \mathbf{v}^l \in \mathbb{R}^{n' \times d/2})$ from \mathbf{T}^l . Next, we carry out attention operation [54] using triplets $(\mathbf{q}^l, \mathbf{k}^s, \mathbf{v}^s)$ and $(\mathbf{q}^s, \mathbf{k}^l, \mathbf{v}^l)$ as inputs by exchanging the key-value pairs from each other. Notably, the last dimension of queries, keys and values from \mathbf{T}^l is lessen from d' to d/2 by projections for the attention, and the attention result for \mathbf{T}^l is re-projected to the dimension of $n' \times d'$, then rearranged to the dimension of $n \times \frac{d}{2}$. Finally, we generate the output token representation of CSTA by concatenating the attention results.

Our CSTA can exploit cross-scale information without additional high overhead. More specifically, computation costs of MHSA and CSTA are as follows:

$$\mathcal{O}(MHSA) = n^2 \cdot d + n \cdot d^2$$

$$\mathcal{O}(CSTA) = (n \cdot n') \cdot d + (n + n') \cdot d^2,$$
(6)

and the computational cost of CSTA is competitive with MHSA because n > n'.

The notion of our CSTA module is computing attention scores across scales in a high-dimensional feature space and explicit reasoning across multi-scale tokens. Thus, our network can utilize recurring patch information across different scales within the input image [41, 43, 50], while conventional MHSA lacks the ability to extract informative cross-scale cues.

3) Multi-branch feature aggregation: As previously shown in Figure 1, we laterally connect the intermediate features extracted from independent branches. In contrast, one can aggregate features without the intermediate fusion as in Figure 3 (a) to generate the SR result. However, such a choice limits the network to utilize its complementary design and also makes it hard to be optimized since the characteristics and computational mechanism of the two branches are highly different. Alternatives of connecting both branches are to unidirectionally pass the information from one branch to another [14] (Figure 3 (b)). This approach

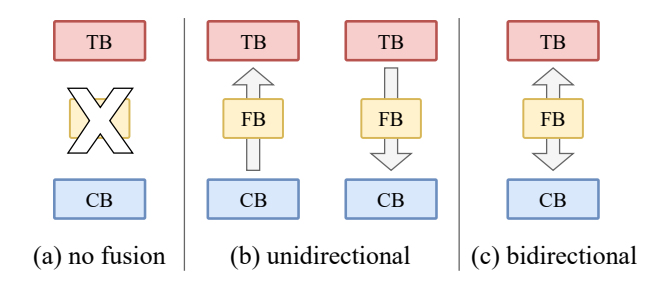


Fig. 3: Variant fusion strategies.

bridges the gap between branches to some extent, but only one side of the branch limitedly receives the fused representation. We aim our lateral fusion to benefit from convolution to transformer and vice versa. Therefore, we propose to fuse both representations and flow it back to both branches (Figure 3 (c)) to let both branches advantageously complement representations from each other.

Figure 4 depicts our Fusion Block. Concretely, given intermediate features T_i and F_i from the *i*th CNN Block and Transformer Block, we aggregate the feature maps by using Fusion Block H_{fuse} as:

$$\mathbf{M}_{i} = H_{fuse}^{i}(\mathbf{rearrange}(\mathbf{T}_{i}) \parallel \mathbf{F}_{i}), \quad 1 \le i \le N, \tag{7}$$

where $\mathbf{M}_i \in \mathbb{R}^{2c \times h \times w}$ denotes the fused features, and rearrange and \parallel represent image-like rearrangement and concatenation, respectively. Here, we empirically determine to concatenate two features rather than element-wise summation for the input of lateral connection (see Appendix). Next, we build our Fusion Block H_{fuse} with 1×1 convolutional blocks to focus on the channel-wise fusion. Except for the last Fusion Block (i.e., i=N), the fused features \mathbf{M}_i are split into two features along the channel dimension, i.e., $\mathbf{M}_i^T \in \mathbb{R}^{c \times h \times w}$ and $\mathbf{M}_i^F \in \mathbb{R}^{c \times h \times w}$, followed by MLP blocks and convolutional blocks, respectively. Then, each fused feature flows back to each branch and is added to the original input feature \mathbf{T}_i and \mathbf{F}_i , individually. The fused feature \mathbf{M}_N at the last Fusion Block takes a single 3×3 convolution layer to resize the channel dimension from 2c to c. The extracted deep residual feature is added to \mathbf{F}_0 , and produce the deep feature \mathbf{F}_{DF} . Subsequently, \mathbf{F}_{DF} is transferred to the final tail module.

C. Tail

For the last step, the aggregated feature \mathbf{F}_{DF} is upscaled and reconstructed through the tail module H_{Tail} and produce the final SR result as:

$$\mathbf{I}_{SR} = H_{Tail}(\mathbf{F}_{DF}). \tag{8}$$

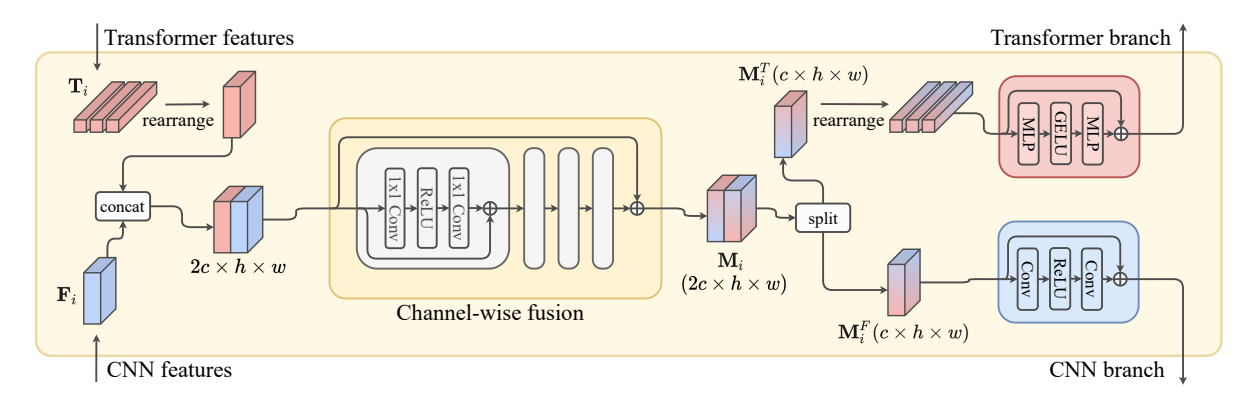


Fig. 4: Our Fusion Block. We concatenate features from two branches, fuse representations with 1×1 convolutions, and bidirectionally transfer the mixed information to the original branches.

 H_{Tail} includes PixelShuffle [49] operation, which upscales feature maps by rearranging channel-wise features to the spatial dimension, followed by a single convolution layer to predict the final SR result.

IV. EXPERIMENTS

In this section, we quantitatively and qualitatively demonstrate the superiority of ACT. Appendix provides additional details and results.

A. Implementation detail

Datasets and evaluation metrics: Following IPT [6], we train our network with the ImageNet dataset [9] to fully utilize the transformer's representation capability. Specifically, we use approximately 1.3M images such that the length of the shortest axis exceeds 400 pixels as ground-truth HR images. Input LR images are generated by downscaling the HR images using the MATLAB impresize function (i.e., bicubic interpolation) as in previous works [6, 32].

Moreover, we evaluate the performance of the SR networks on conventional SR benchmark datasets: Set5 [2], Set14 [63], B100 [37], Urban100 [23], and Manga109 [39]. The experimental results are evaluated with two metrics, namely peak signal-to-noise ratio (PSNR) and structural similarity (SSIM), on the Y channel in YCbCr color space following the baselines [6, 33, 64].

Hyper-parameter setting: We have four CNN Blocks in the CNN branch and four Transformer Blocks in the transformer branch (i.e., N=4). Each CNN Block includes 12 RCAB modules with channel size c=64. We use d=576, and the expansion ratio r inside the FFN module is set to 4. For the Fusion Block, we stack four 1×1 residual blocks [21].

During the training, input LR patches are fixed to 48×48 , and the token size is 3×3 (i.e., t=3). We also use conventional data augmentation techniques, such as rotation (90°, 180°, and 270°) and horizontal flipping. The large token size t', stride s', and d' for the CSTA module are set to 6, 3, and 1152, respectively. Moreover, we use Adam optimizer [29] to train our network and minimize the L_1 loss following previous studies [6, 42, 64]. We train our network for 150 epochs with a batch size of 512. The initial learning rate is 10^{-4} ($\beta_1=0.9$, $\beta_2=0.999$, and $\epsilon=10^{-8}$) and we reduce the rate by half every 50 epochs. We implement our model using the PyTorch framework with eight NVIDIA A100 GPUs.

B. Ablation study

We provide several ablation studies to verify our design choices, effectiveness, and superiority of the proposed modules.

1) Impact of positional embeddings: Unlike high-level vision tasks (e.g., classification), the transformer in SR utilizes a relatively small patch size and is not invariant to the order of token embeddings since tokens are rearranged back into the original position to generate an HR image [36]; thus lessening the necessity of the positional embeddings. To confirm, we train two types of SR networks by using 1) MHSA instead of CSTA and removing the CNN branch (i.e., standard ViT [11]) and 2) our ACT. The networks are trained with and without learnable positional embeddings [4,6,11], and results are provided in Table I. We observe that transformer without positional embeddings does not degrade the performance and even shows slightly better performance (approximately 0.03dB) than the transformer trained with the positional embeddings. According to our observation, we do not use positional embeddings in the remainder of our experiments.

| | | PSNR |
|--------------|----|--------------------|
| Method | PE | Set5/Set14 |
| Standard ViT | o | 38.31/34.29 |
| Standard ViT | x | 38.33/34.33 |
| ACT (Ours) | o | 38.43/34.57 |
| ACT (Ours) | x | 38.46/34.60 |

TABLE I: Ablation on the impact of the positional embeddings for the SR task. PE indicates positional embeddings.

| | Single- | stream | Two-stream | | | | |
|---------------|--------------|--------------|--------------|--------------|--------------|-----------------------|--|
| Component | | | | | | | |
| Transformer | О | X | o | 0 | 0 | o | |
| CNN | X | o | О | o | o | o | |
| Fusion | x | X | x | $T\toC$ | $C \to T$ | $T \leftrightarrow C$ | |
| Param. | 32.8M | 4.3M | 36.6M | 37.4M | 45.1M | 45.3M | |
| Performance | | | | | | | |
| Set5 [2] | 38.33/0.9619 | 38.20/0.9615 | 38.28/0.9618 | 38.35/0.9620 | 38.33/0.9620 | 38.38/0.9621 | |
| Set14 [63] | 34.33/0.9240 | 34.21/0.9224 | 34.32/0.9232 | 34.38/0.9239 | 34.44/0.9240 | 34.45/0.9243 | |
| B100 [37] | 32.46/0.9037 | 32.41/0.9030 | 32.45/0.9036 | 32.49/0.9040 | 32.50/0.9041 | 32.53/0.9044 | |
| Urban100 [23] | 33.78/0.9423 | 33.24/0.9381 | 33.49/0.9404 | 33.66/0.9413 | 33.86/0.9427 | 33.93/0.9431 | |
| Manga109 [39] | 39.48/0.9795 | 39.46/0.9794 | 39.56/0.9795 | 39.71/0.9797 | 39.77/0.9800 | 39.85/0.9801 | |

TABLE II: Ablation experiments about various architectural design related to the proposed method. T and C means Transformer and CNN branches respectively. \rightarrow indicates unidirectional flow from left to right, and \leftrightarrow indicates bidirectional flow. We report PSNR and SSIM on the left and right side of the slash.

- 2) Impact of fusing strategies: We ablate various architectural choices related to the proposed multi-stream network and report the evaluation results on numerous benchmark datasets in Table II. Specifically, we conduct experiments on each branch and fusion strategies. First, the single-stream network with only the transformer branch performs better than the relatively lightweight single-stream network with the CNN branch, especially for the challenging urban dataset, due to the large model capacity of the transformer. Next, we observe that the performance of the two-stream network without Fusion Block consistently drops for all datasets due to extremely separated pathways. However, the performance is largely improved when intermediate features are unidirectionally fused, while exceptional case, such as the fusion from the transformer to CNN branch ($T \rightarrow C$) exists (-0.12 dB than the single transformer branch in the urban dataset). Finally, the proposed bidirectional fusion between the CNN and transformer features ($T \leftrightarrow C$) shows the best performance over the entire fusion strategy. The experimental results show that the transformer and CNN branches contain complementary information, and the intermediate bidirectional fusion is necessary for the satisfactory restoration results.
- 3) Impact of CSTA: In Table III, we evaluate the effectiveness of the proposed cross-scale token attention mechanism with various viewpoints.

MHSA vs. CSTA: First, we compare our CSTA against the standard MHSA in Table III (a). More specifically, we additionally train our ACT by replacing all CSTA/MHSA with MHSA/CSTA (i.e., 'MHSA only' and 'CSTA only'). The comparison between 'MHSA only' and 'MHSA + CSTA' indicates that CSTA largely boosts performance with a small number of additional parameters (+ 0.7M). Moreover, the result of 'CSTA only' indicates that CSTA alone cannot cover the role of MHSA capturing self-similarity within the same scale (performs better than 'MHSA only' but lower than 'MHSA + CSTA').

Impact of the number of large tokens: Next, we conduct experiments to observe the impact of the large tokens and their efficiency in Table III (b). Specifically, we vary the sequence length of large token (i.e., n') of \mathbf{T}^l by

| | | PSNR |
|-------------|--------|----------------|
| Method | Param. | Set14/Urban100 |
| MHSA only | 45.3M | 34.45/33.93 |
| MHSA + CSTA | 46.0M | 34.60/34.07 |
| CSTA only | 46.7M | 34.51/33.92 |

| CSTA | x | | 0 | |
|-----------------------|-------|--------------------|-------|--------------|
| Stride (s') | | 5 | 4 | 3 |
| # large tokens (n') | | 81 | 121 | 225 |
| FLOPs | 22.2G | 21.4G 34.51 | 21.6G | 22.2G |
| PSNR (Set14) | 34.45 | | 34.55 | 34.60 |

| # scales | PSNR |
|---------------|----------------|
| (token sizes) | Set14/Urban100 |
| 1 (3) | 34.45/33.93 |
| 2 (3, 6) | 34.60/34.07 |
| 3 (3, 6, 12) | 34.52/33.95 |

CSTA alone.

(a) MHSA vs. CSTA. Utilizing both atten- (b) Effect of the number of large tokens n'. CSTA (c) Effect of various scaled totions is consistently better than MHSA or consistently and efficiently boost performance.

kens. CSTA with two scales performs best.

TABLE III: Ablation experiments on CSTA module. We demonstrate the effectiveness of our proposed CSTA on various aspects.

controlling the stride s'. The results show that our CSTA module even with a small number of large tokens (n' = 81)efficiently outperforms conventional self-attention without cross-attention (i.e., MHSA) by 0.06dB. Furthermore, performance improvement is remarkable when we increase the number of large tokens with a small overhead in terms of FLOPs. This experimental result demonstrates that CSTA can efficiently exploit informative cross-scale features with larger tokens.

Impact of more token scales: Finally, we conduct experiments to observe whether performing CSTA with more token sizes benefits the network or not in Table III (c). Doing so, we embed three sizes (3, 6, and 12) of tokens with similar overall computational cost to the CSTA module. The comparison between two token scales and three token scales shows that cross attention with an additional larger scale rather drops the performance. Since the number of recurring patches decreases as scale increases [68], we observe that exploiting self-similar patches across proper scales is more effective than solely performing certain types of attention or adding various scales.

4) Feature visualization: We visualize feature maps to analyze and compare the feature from each branch. To do so, we channelwisely average the absolute value of the output features from the last blocks for each branch (i.e., T_4 and F_4) and normalize each of them similar to [24]. We rearrange tokens into imagelike features for visualization. The visualized result in Figure 5 reveals that the roles of the transformer and CNN branches are different. First, both branches provide minimal attention to the flat low-frequency area (e.g., sky). However, the output feature from the transformer branch concentrates on recovering tiny and high-frequency texture details while producing a certain amount of blurry and checkerboard artifacts due to the tokenization. Moreover, our transformer branch leverages multi-scale representations by the CSTA module; thus, the transformer focuses on the small version of recurring patches within the image interestingly (e.g., upper side window in the right example). In contrast, the CNN branch focuses on recovering the sharp and strong edges, which the transformer branch fails to capture. This observation indicates that the network endowed independent roles for each pathway such that two branches complement each other.

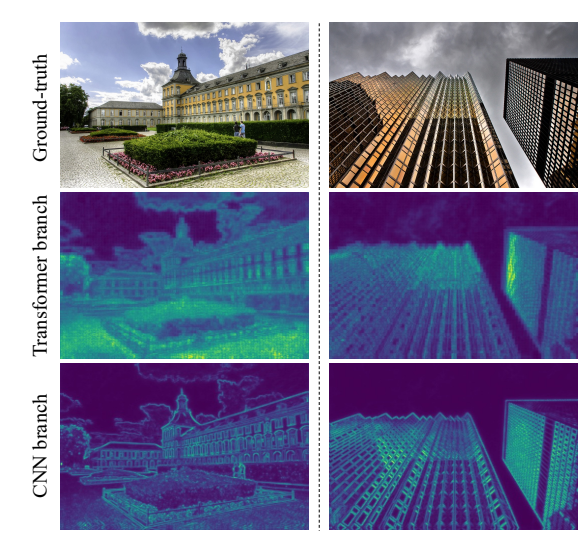


Fig. 5: Feature map visualizations of transformer branch and CNN branch.

C. SR results

1) Quantitative evaluation: In Table IV, we quantitatively compare our ACT for $\times 2$, $\times 3$, and $\times 4$ SR tasks with the 9 state-of-the-art SR networks: EDSR [33], RCAN [64], RNAN [65], SAN [8], HAN [42], IGNN [66], NLSA [40], IPT [6], and SwinIR [32]. Notably, IPT [6] and SwinIR [32] are the recently developed transformerbased methods. We also report the test-time self-ensembling-based results following the baselines [32, 33, 42, 64] to further improve the performance, and ACT+ indicates the approach with the self-ensemble [33]. Compared with all previous works, ACT and ACT+ achieve the best or the second-best performance in terms of PSNR and SSIM

| | | | Set | 5 [2] | Set1 | 4 [63] | B100 | 0 [37] | Urban | 100 [23] | Manga | 109 [39] |
|-------------|------------|-------------------|-------|--------|-------|--------|-------|--------|-------|----------|-------|----------|
| Method | Scale | Component | PSNR | SSIM | PSNR | SSIM | PSNR | SSIM | PSNR | SSIM | PSNR | SSIM |
| EDSR [33] | $\times 2$ | CNN | 38.11 | 0.9602 | 33.92 | 0.9195 | 32.32 | 0.9013 | 32.93 | 0.9351 | 39.10 | 0.9773 |
| RCAN [64] | $\times 2$ | CNN | 38.27 | 0.9614 | 34.12 | 0.9216 | 32.41 | 0.9027 | 33.34 | 0.9384 | 39.44 | 0.9786 |
| RNAN [65] | $\times 2$ | CNN | 38.17 | 0.9611 | 33.87 | 0.9207 | 32.32 | 0.9014 | 32.73 | 0.9340 | 39.23 | 0.9785 |
| SAN [8] | $\times 2$ | CNN | 38.31 | 0.9620 | 34.07 | 0.9213 | 32.42 | 0.9028 | 33.10 | 0.9370 | 39.32 | 0.9792 |
| HAN [42] | $\times 2$ | CNN | 38.27 | 0.9614 | 34.16 | 0.9217 | 32.41 | 0.9027 | 33.35 | 0.9385 | 39.46 | 0.9785 |
| IGNN [66] | $\times 2$ | CNN | 38.24 | 0.9613 | 34.07 | 0.9217 | 32.41 | 0.9025 | 33.23 | 0.9383 | 39.35 | 0.9786 |
| NLSA [40] | $\times 2$ | CNN | 38.34 | 0.9618 | 34.08 | 0.9231 | 32.43 | 0.9027 | 33.42 | 0.9394 | 39.59 | 0.9789 |
| IPT [6] | $\times 2$ | ViT [11] | 38.37 | | 34.43 | | 32.48 | | 33.76 | - | | - |
| SwinIR [32] | $\times 2$ | Swin [35] + CNN | 38.42 | 0.9623 | 34.46 | 0.9250 | 32.53 | 0.9041 | 33.81 | 0.9427 | 39.92 | 0.9797 |
| ACT (Ours) | $\times 2$ | ViT [11] + CNN | 38.46 | 0.9626 | 34.60 | 0.9256 | 32.56 | 0.9048 | 34.07 | 0.9443 | 39.95 | 0.9804 |
| ACT+ (Ours) | $\times 2$ | ViT [11] + CNN | 38.53 | 0.9629 | 34.68 | 0.9260 | 32.60 | 0.9052 | 34.25 | 0.9453 | 40.11 | 0.9807 |
| EDSR [33] | $\times 3$ | CNN | 34.65 | 0.9280 | 30.52 | 0.8462 | 29.25 | 0.8093 | 28.80 | 0.8653 | 34.17 | 0.9476 |
| RCAN [64] | $\times 3$ | CNN | 34.74 | 0.9299 | 30.65 | 0.8482 | 29.32 | 0.8111 | 29.09 | 0.8702 | 34.44 | 0.9499 |
| SAN [8] | $\times 3$ | CNN | 34.75 | 0.9300 | 30.59 | 0.8476 | 29.33 | 0.8112 | 28.93 | 0.8671 | 34.30 | 0.9494 |
| HAN [42] | $\times 3$ | CNN | 34.75 | 0.9299 | 30.67 | 0.8483 | 29.32 | 0.8110 | 29.10 | 0.8705 | 34.48 | 0.9500 |
| IGNN [66] | $\times 3$ | CNN | 34.72 | 0.9298 | 30.66 | 0.8484 | 29.31 | 0.8105 | 29.03 | 0.8696 | 34.39 | 0.9496 |
| NLSA [40] | $\times 3$ | CNN | 34.85 | 0.9306 | 30.70 | 0.8485 | 29.34 | 0.8117 | 29.25 | 0.8726 | 34.57 | 0.9508 |
| IPT [6] | ×3 | ViT [11] | 34.81 | | 30.85 | | 29.38 | | 29.38 | | | - |
| SwinIR [32] | $\times 3$ | Swin $[35]$ + CNN | 34.97 | 0.9318 | 30.93 | 0.8534 | 29.46 | 0.8145 | 29.75 | 0.8826 | 35.12 | 0.9537 |
| ACT (Ours) | $\times 3$ | ViT [11] + CNN | 35.03 | 0.9321 | 31.08 | 0.8541 | 29.51 | 0.8164 | 30.08 | 0.8858 | 35.27 | 0.9540 |
| ACT+ (Ours) | $\times 3$ | ViT [11] + CNN | 35.09 | 0.9325 | 31.17 | 0.8549 | 29.55 | 0.8171 | 30.26 | 0.8876 | 35.47 | 0.9548 |
| EDSR [33] | $\times 4$ | CNN | 32.46 | 0.8968 | 28.80 | 0.7876 | 27.71 | 0.7420 | 26.64 | 0.8033 | 31.02 | 0.9148 |
| RCAN [64] | $\times 4$ | CNN | 32.63 | 0.9002 | 28.87 | 0.7889 | 27.77 | 0.7436 | 26.82 | 0.8087 | 31.22 | 0.9173 |
| RNAN [65] | $\times 4$ | CNN | 32.49 | 0.8982 | 28.83 | 0.7878 | 27.72 | 0.7421 | 26.61 | 0.8023 | 31.09 | 0.9149 |
| SAN [8] | $\times 4$ | CNN | 32.64 | 0.9003 | 28.92 | 0.7888 | 27.78 | 0.7436 | 26.79 | 0.8068 | 31.18 | 0.9169 |
| HAN [42] | $\times 4$ | CNN | 32.64 | 0.9002 | 28.90 | 0.7890 | 27.80 | 0.7442 | 26.85 | 0.8094 | 31.42 | 0.9177 |
| IGNN [66] | $\times 4$ | CNN | 32.57 | 0.8998 | 28.85 | 0.7891 | 27.77 | 0.7434 | 26.84 | 0.8090 | 31.28 | 0.9182 |
| NLSA [40] | $\times 4$ | CNN | 32.59 | 0.9000 | 28.87 | 0.7891 | 27.78 | 0.7444 | 26.96 | 0.8109 | 31.27 | 0.9184 |
| IPT [6] | $\times 4$ | ViT [11] | 32.64 | | 29.01 | | 27.82 | | 27.26 | - | | |
| SwinIR [32] | $\times 4$ | Swin [35] + CNN | 32.92 | 0.9044 | 29.09 | 0.7950 | 27.92 | 0.7489 | 27.45 | 0.8254 | 32.03 | 0.9260 |
| ACT (Ours) | $\times 4$ | ViT [11] + CNN | 32.97 | 0.9031 | 29.18 | 0.7954 | 27.95 | 0.7507 | 27.74 | 0.8305 | 32.20 | 0.9267 |
| ACT+ (Ours) | $\times 4$ | ViT [11] + CNN | 33.04 | 0.9041 | 29.27 | 0.7968 | 28.00 | 0.7516 | 27.92 | 0.8332 | 32.44 | 0.9282 |

TABLE IV: Quantitative comparison of the proposed method with numerous state-of-the-art SR methods. The best and the second-best values are highlighted with red and blue color, respectively.

for all scale factors. In particular, our method substantially outperforms IPT [6], which is recognized as the first transformer-based restoration approach, through the proposed multi-scale feature extraction as well as the effective hybridized architecture of the CNN and transformer. Moreover, the performance improvement over SwinIR [32] is especially large for the Urban100 dataset [23] (more than 0.3dB PSNR gain for all scale factors) with the high patch-recurrence in the dataset, indicating that our CSTA module successfully exploits multi-scale features.

2) Qualitative evaluation: We also provide a qualitative comparison with the existing SR methods. Figure 6 shows that our method obtains more accurately recovered details than the conventional methods. Specifically, the restoration result of the image "MisutenaideDaisy" demonstrates that our method can generate more human-readable characters than other existing methods. Moreover, take "barbara" as an example, baseline methods have generated sharp edges/patterns despite being far from the ground-truth structure. By contrast, our method properly reconstructs the main structure without losing the high-frequency details. The result of "img092" which contains urban scene also shows that most of the conventional methods fail to recover the structure and produce blurry results. Meanwhile, our method alleviates blurring artifacts and accurately reconstructs correct contents. The above observation indicates the general superiority of the proposed method in recovering sharp and accurate details.

D. Model size analysis

Finally, we compare the number of network parameters and floating-point operations (FLOPs) of various SR methods in Table V. Our ACT shows the best SR results as in Table IV, while the number of parameters and operational costs is competitive in comparison with conventional approaches, including IPT [6] and SwinIR [32].



Fig. 6: Visual comparison of the proposed method with various methods for $\times 4$ SR task. Our method restores sharp and complicated structures more accurately.

| Measure | EDSR [33] | RCAN [64] | NLSA [40] | IPT [6] | SwinIR [32] | ACT (Ours) |
|---------|-----------|-----------|-----------|---------|-------------|------------|
| Param. | 43M | 16M | 44M | 114M | 12M | 46M |
| FLOPs | 116G | 37G | 125G | 35G | 29G | 22G |

TABLE V: Comparison of the proposed method's resources with state-of-the-art SR methods. Ours shows comparable hardware consumption for both network parameters and operation counts with better performance.

The comparison demonstrates an effective trade-off between the performance and model complexity of our proposed method.

V. DISCUSSION AND CONCLUSION

We have proposed a novel SR network, namely ACT, which combines transformers and CNNs, and the proposed network architecture interacts and complements representations. Moreover, we have presented an efficient multiscale feature learning module, which exploits multi-scale feature maps within a transformer. The effectiveness of the proposed method has been extensively demonstrated with various experiments under numerous benchmark SR datasets, and ACT records the state-of-the-art SR performance in terms of quantitative and qualitative comparisons.

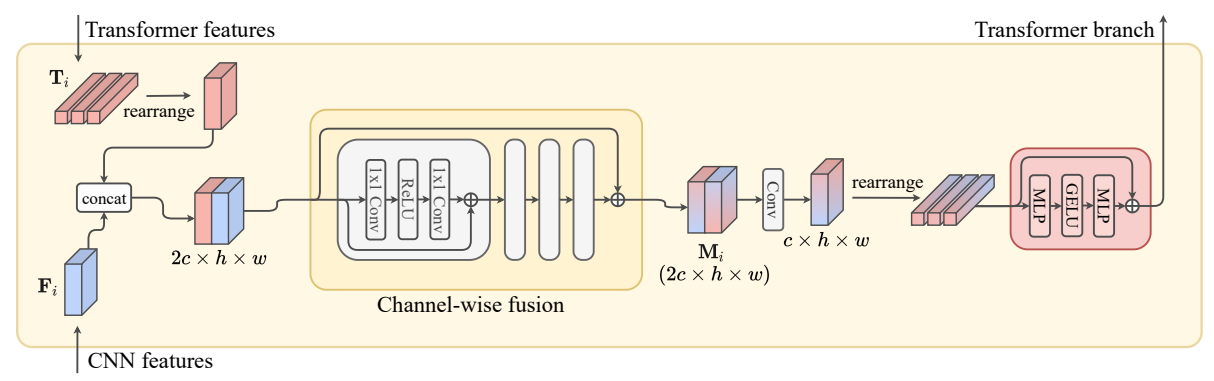
Although the proposed ACT effectively exploits both CNN and multi-scale transformer features, our current model complexity still remains quadratic to the sequence length, which possibly serves as a critical bottleneck for a real-world application including video restoration. Therefore, we plan to further extend our model to be more efficient by applying the recent techniques such as linear transformer [55] or sparse tokenization [45, 47] in the future.

APPENDIX

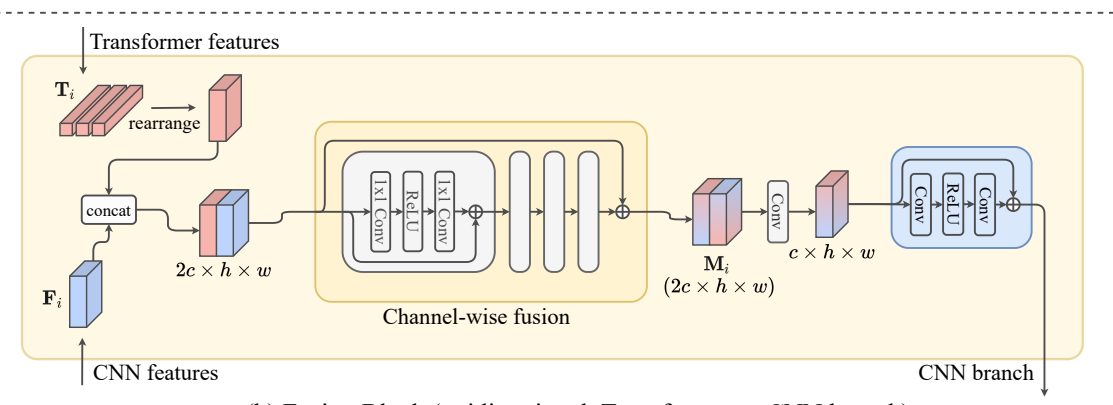
In this appendix, we provide additional details, experimental settings, and results of our proposed method. We first describe the details of the proposed Fusion Block in Section A and CSTA in Section B. Next, Section C gives more results about the model size analysis in the main manuscript (*i.e.*, section 4.4). We also show the applicability of our approach to another image restoration task (*i.e.*, JPEG artifact removal) in Section D. Finally, we provide more visual results of feature visualization and qualitative comparisons in Section E and Section F, respectively.

A. Fusion Block

In this section, we present detailed configuration and additional results of our Fusion Block.



(a) Fusion Block (unidirectional, CNN to transformer branch)



(b) Fusion Block (unidirectional, Transformer to CNN branch)

Fig. 7: Illustration of the unidirectional Fusion Blocks.

- 1) Settings for the ablation: We elaborate the detailed settings of our fusion strategies in the manuscript. For the ablation experiment without the intermediate fusion (3rd column in Table II), we simply concatenate the output features T_4 and F_4 from the separated branches, and pass them to the tail module. For the experiments with unidirectional flow (4th and 5th columns in Table II), we do not split the feature M_i into two. Instead, we reduce the channel dimension from 2c to c with a single convolution layer and transfer it to the branch chosen to receive the fused representation (see Figure 7 (a) (b)).
- 2) Experiment on lateral connection: Since the dimension of feature from the CNN branch and image-likely rearranged feature from the transformer branch are the same (i.e., $c \times h \times w$), one can laterally connect two features with elementwise summation rather than concatenation in Equation 7. We compare the performance of different lateral connection choices in Table VI, and observe that concatenation gives slightly better results than summation.

| | | PSNR |
|------------|---------------|-----------------------------------|
| Method | Lateral | Set14/Urban100 |
| ACT ACT | sum concat | 34.57/34.05 34.60/34.07 |

TABLE VI: Comparison on different lateral connections of two branches in our Fusion Block ($\times 2$ SR).

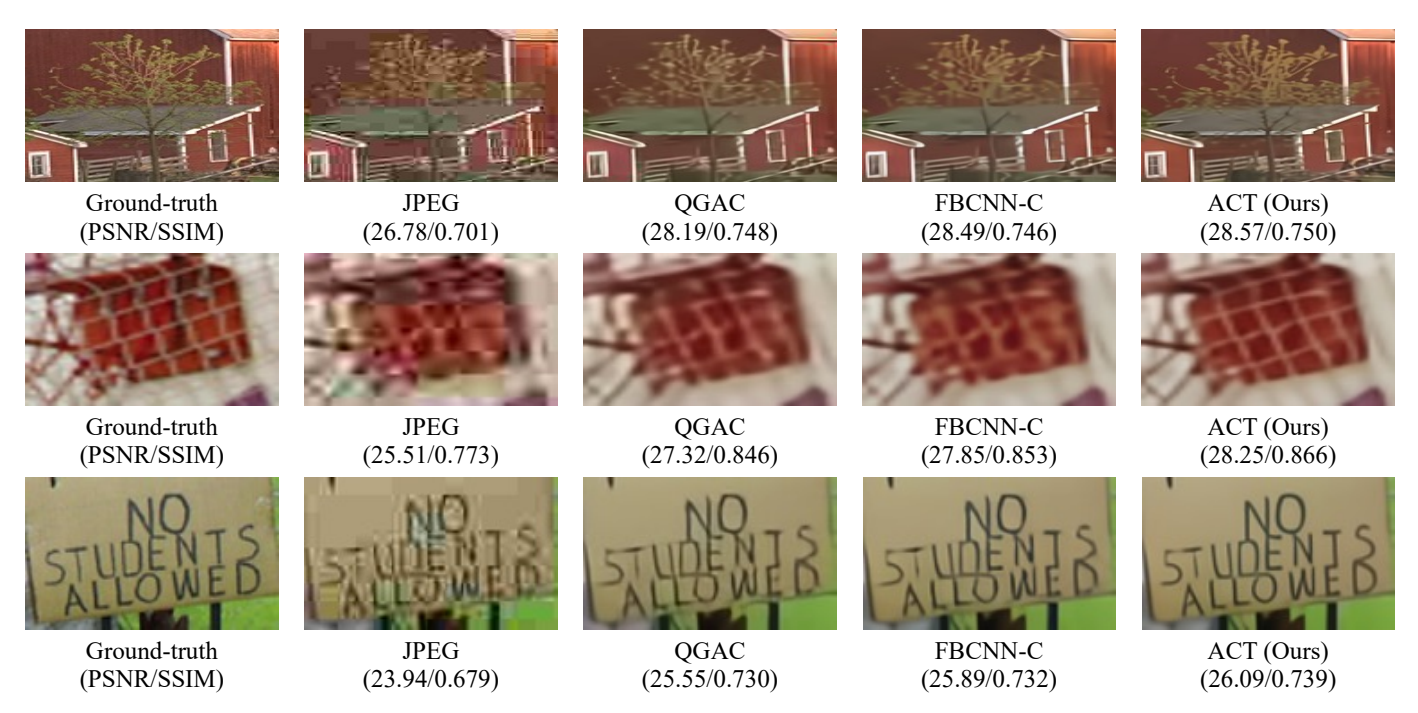


Fig. 8: Visual comparison of our ACT against state-of-the-art color JPEG artifact removal methods [13, 26] with quality factor of 10. Our ACT removes the artifacts better than the baselines.

B. Cross-Scale Token Attention

In this section, we provide pseudocode of the CSTA procedure and experimental settings for our ablation.

- 1) Pseudocode of CSTA: Algorithm 1 provides the pseudocode of CSTA for better understanding. In particular, we split the hidden dimension of \mathbf{T} into two, and directly utilize \mathbf{T}^a for \mathbf{T}^s while reformulating \mathbf{T}^b to acquire \mathbf{T}^l as elaborated in the main manuscript. It is worth noting that such rearrangement is similar to the soft-split introduced in T2T-ViT [61] in that the tokens are re-structurized by overlapping. Unlike soft-split, we rearrange only a part of the hidden dimension within the token \mathbf{T} with a larger token size to perform the cross-attention efficiently, and the notion of the rearrangement is to acquire fruitful larger tokens (patches) to exploit the recurring patches across different scales within the input image.
- 2) Settings for the ablation: We elaborate details about the "Impact of more token scales" experiment in our ablation on CSTA in the main manuscript. Specifically, we demonstrate how we perform cross-attention by introducing three different token scales (3rd row in Table III (c)). To enable our network to enjoy patch-recurrence across various scales while maintaining similar computational cost, we first split the input token $\mathbf{T} \in \mathbb{R}^{n \times d}$ into four tokens $\{\mathbf{T}_i\}_{i=1}^4 \in \mathbb{R}^{n \times d/4}$ before cross-attention. Then, we rearrange \mathbf{T}_2 and \mathbf{T}_4 with token size of 6×6 and 12×12 , respectively, with the same strides of 3, while \mathbf{T}_1 and \mathbf{T}_3 keep their token size of 3×3 . We perform two independent cross-attention using $(\mathbf{T}_1, \mathbf{T}_2)$ and $(\mathbf{T}_3, \mathbf{T}_4)$ pair as elaborated in the main manuscript. Consequently, the network can utilize multi-scale information across various scales. Lastly, we re-concatenate four tokens into one after rearranging token \mathbf{T}_2 and \mathbf{T}_4 to include a token size of 3×3 .

C. Model Size Analysis

For model size analysis in Table V, we count FLOPs for 48×48 image following IPT [6] using the open source. ¹ Moreover, we compare the runtime of our model with recently proposed transformer-based SR methods [6, 32]. We average 5 runs on the same setting as in Table V with Ryzen 2950X CPU and NVIDIA 2080 Ti, and the result in Table VII shows that ours is competitive in runtime.

| IPT [6] | SwinIR [32] | ACT (Ours) |
|---------|-------------|------------|
| 0.586s | 0.528s | 0.566s |

TABLE VII: Runtime comparison.

¹https://github.com/facebookresearch/fvcore

| Dataset | QF | JPEG | QGAC [13] | FBCNN-C [26] | ACT (Ours) |
|--------------|----|-------------------|----------------------------------|-------------------|-------------------|
| | 10 | 25.69/0.743/24.20 | 27.62/0.804/27.43 | 27.77/0.803/27.51 | 27.94/0.808/27.63 |
| L IV/E1 [40] | 20 | 28.06/0.826/26.49 | 29.88/0.868/29.56 | 30.11/0.868/29.70 | 30.39/0.874/29.96 |
| LIVE1 [48] | 30 | 29.37/0.861/27.84 | 31.17/0.896/30.77 | 31.43/0.897/30.92 | 31.77/0.902/31.26 |
| | 40 | 30.28/0.882/28.84 | 32.05/0.912/31.61 | 32.34/0.913/31.80 | 32.70/0.917/32.16 |
| | 10 | 25.84/0.741/24.13 | 27.74/0.802/27.47 | 27.85/0.799/27.52 | 27.84/0.800/27.46 |
| DCDC500 [20] | 20 | 28.21/0.827/26.37 | 30.01/ <mark>0.869</mark> /29.53 | 30.14/0.867/29.56 | 30.20/0.868/29.58 |
| BSDS500 [38] | 30 | 29.57/0.865/27.72 | 31.33/0.898/30.70 | 31.45/0.897/30.72 | 31.51/0.897/30.77 |
| | 40 | 30.52/0.887/28.69 | 32.25/0.915/31.50 | 32.36/0.913/31.52 | 32.41/0.914/31.56 |
| | 10 | 29.44/0.757/28.53 | 32.06/ <mark>0.816</mark> /32.04 | 32.18/0.815/32.15 | 32.20/0.816/32.17 |
| ICB [46] | 20 | 32.01/0.806/31.11 | 34.13/0.843/34.10 | 34.38/0.844/34.34 | 34.50/0.844/34.46 |
| | 30 | 33.20/0.831/32.35 | 35.07/0.857/35.02 | 35.41/0.857/35.35 | 35.61/0.859/35.55 |
| | 40 | 33.95/0.840/33.14 | 32.25/ <mark>0.915</mark> /31.50 | 36.02/0.866/35.95 | 36.21/0.868/36.13 |

TABLE VIII: PSNR/SSIM/PSNRB comparison of different state-of-the-art methods on color JPEG artifact removal. Our ACT shows competitive performance over baselines despite a lack of hand-crafted task-specific architectural design. Performances for the baselines are borrowed from [26].

D. Applicability to other Image Restoration Tasks

We propose ACT to solve the SR problem, however, ACT can be easily integrated with other image restoration tasks without bells and whistles. We investigate the applicability of our network to a challenging restoration task; color JPEG artifact removal. To do so, we only modify the tail part of the network to include a single convolutional layer while discarding PixelShuffle upsampler [49] and remain other components as same as SR architecture. We train our network with same training configurations for SR, and the training patch size is 48×48 . We compare our ACT with the state-of-the-art color JPEG artifact removal methods including QGAC [13] and FBCNN-C [26] for quality factors of 10, 20, 30, and 40. We evaluate performance on the LIVE1 [48], BSDS500 [38], and ICB [46] datasets with three different metrics including PSNR, SSIM, and PSNR-B values following the baselines [13, 26]. We report the quantitative comparison in Table VIII. As shown in the table, our ACT shows promising results despite lacking task-specific architectural design. Moreover, we visually compare our method against the baselines in Figure 8. Our ACT more accurately recovers the corrupted images including natural scenes, sharp textures, and characters. This result implies the possibility of applying our ACT to various restoration tasks as similar to the recent image restoration transformers [6, 32, 58].

E. Feature Visualization

In Figure 9, we provide more feature visualizations to understand the role of the two branches.

F. Additional Qualitative Results

To further demonstrate the superiority of our proposed method, we provide more visual comparisons with 6 state-of-the-art SR methods: EDSR [33], RCAN [64], HAN [42], NLSA [40], IPT [6], and SwinIR [32]. The visual comparisons are shown in Figure 10 and Figure 11.

Algorithm 1: Pseudocode of CSTA in a PyTorch-like style.

```
\# b, n, d: batch size, number of tokens, and hidden dimension of {f T}
\# n', d': number of tokens and hidden dimension of \mathbf{T}^l directly after
acquiring large tokens from \mathbf{T}^b by rearrangement
\# h, w: height and width of patches
import torch
import torch.nn.functional as F
def CSTA(T):
   # split \mathbf{T} (b \times n \times d) into \mathbf{T}^a and \mathbf{T}^b
   T_a, T_b = torch.split(T, d//2, dim=2)
   # acquire \mathbf{T}^s from \mathbf{T}^a
   T_s = T_a
   \# acquire \mathbf{T}^l from \mathbf{T}^b by rearrangement
   T_l = F.fold(T_b, output_size=(h, w), kernel_size=token_size,
   stride=token size)
   T_l = F.unfold(T_l, kernel_size=token_size*2, stride=token_size)
   # project tokens into query, key, and value
   T_l = mlp_blk_before_attn(T_l) \# reduce dimension from d' to d/2
   q_1, k_1, v_1 = project(T_1)
   q_s, k_s, v_s = project(T_s)
   # perform cross attention
   T_l = attention(query=q_l, key=k_s, value=v_s)
   T_s = attention(query=q_s, key=k_l, value=v_l)
   \sharp increase hidden dimension of \mathbf{T}^l from d/2 to d'
   T_l = mlp_blk_after_attn(T_l)
   # rearrange \mathbf{T}^l from (b \times n' \times d') to (b \times n \times (d/2))
   T_l = F.fold(T_l, output_size=(h, w), kernel_size=token_size*2,
   stride=token size)
   T_l = F.unfold(T_l, kernel_size=token_size, stride=token_size)
   # concatenate \mathbf{T}^s and \mathbf{T}^l into \mathbf{T} (b \times n \times d)
   T = torch.cat((T_s, T_l), dim=2)
```

return T



Fig. 9: Feature map visualizations of transformer branch and CNN branch. Brighter color indicates higher value.

REFERENCES

- [1] Ba, J.L., Kiros, J.R., Hinton, G.E.: Layer normalization. arXiv preprint arXiv:1607.06450 (2016) 4
- [2] Bevilacqua, M., Roumy, A., Guillemot, C., Alberi-Morel, M.L.: Low-complexity single-image super-resolution based on nonnegative neighbor embedding. In: Proceedings of the British Machine Vision Conference (BMVC) (2012) 6, 7, 9
- [3] Cao, J., Li, Y., Zhang, K., Van Gool, L.: Video super-resolution transformer. arXiv preprint arXiv:2106.06847 (2021) 1, 2
- [4] Carion, N., Massa, F., Synnaeve, G., Usunier, N., Kirillov, A., Zagoruyko, S.: End-to-end object detection with transformers. In: Proceedings of the European Conference on Computer Vision (ECCV) (2020) 1, 2, 7
- [5] Chen, C.F., Fan, Q., Panda, R.: Crossvit: Cross-attention multi-scale vision transformer for image classification. In: Proceedings of the IEEE International Conference on Computer Vision (ICCV) (2021) 2
- [6] Chen, H., Wang, Y., Guo, T., Xu, C., Deng, Y., Liu, Z., Ma, S., Xu, C., Xu, C., Gao, W.: Pre-trained image processing transformer. In: Proceedings of the IEEE Conference on Computer Vision and Pattern Recognition (CVPR) (2021) 1, 2, 3, 4, 6, 7, 8, 9, 10, 12, 13
- [7] Chen, Y., Dai, X., Chen, D., Liu, M., Dong, X., Yuan, L., Liu, Z.: Mobile-former: Bridging mobilenet and transformer. arXiv preprint arXiv:2108.05895 (2021) 3
- [8] Dai, T., Cai, J., Zhang, Y., Xia, S.T., Zhang, L.: Second-order attention network for single image super-resolution. In: Proceedings of the IEEE Conference on Computer Vision and Pattern Recognition (CVPR) (2019) 2, 8, 9

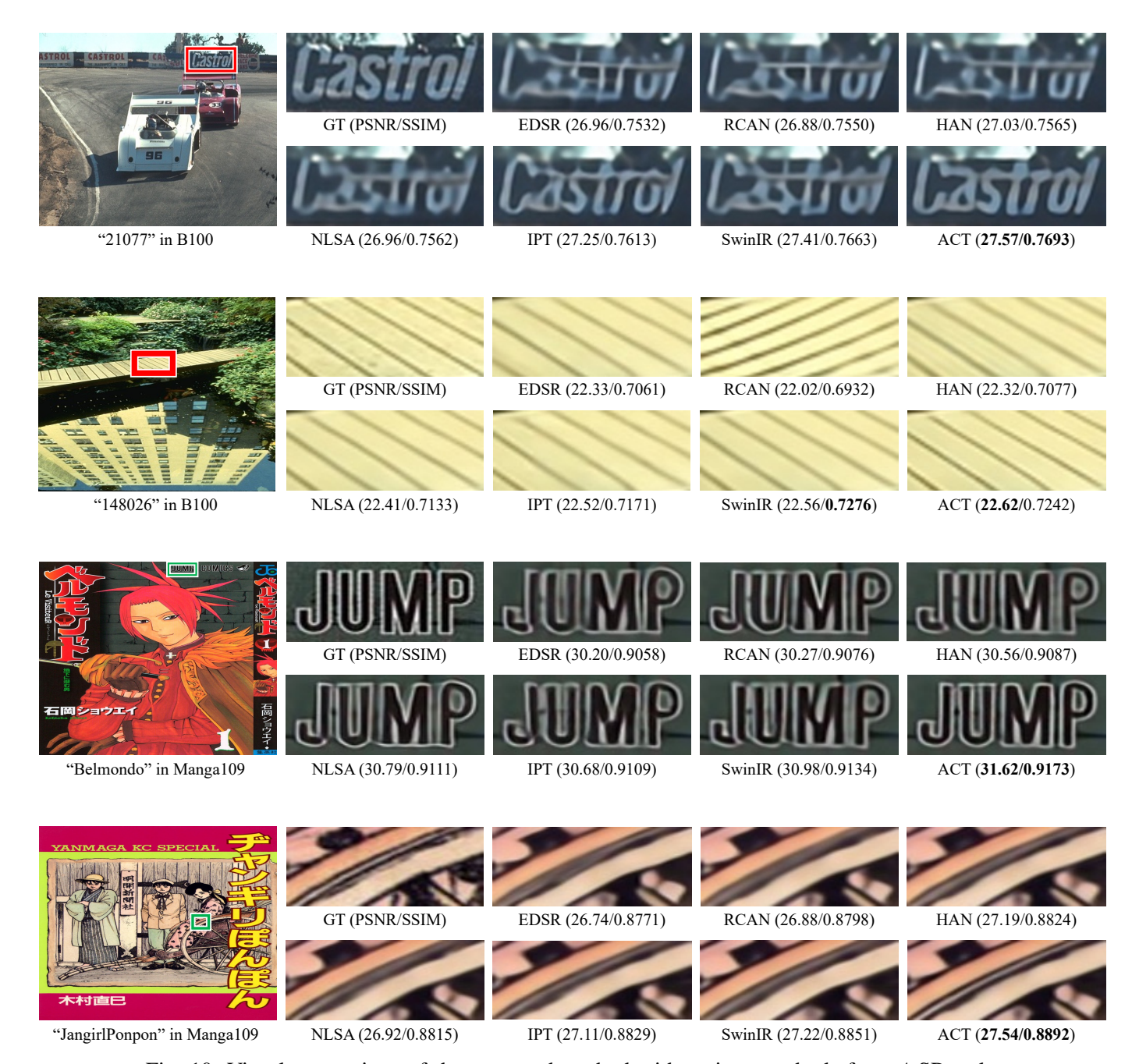


Fig. 10: Visual comparison of the proposed method with various methods for $\times 4$ SR task.

- [9] Deng, J., Dong, W., Socher, R., Li, L.J., Li, K., Fei-Fei, L.: Imagenet: A large-scale hierarchical image database. In: Proceedings of the IEEE Conference on Computer Vision and Pattern Recognition (CVPR) (2009) 6
- [10] Dong, C., Loy, C.C., He, K., Tang, X.: Image super-resolution using deep convolutional networks. IEEE Transactions on Pattern Analysis and Machine Intelligence (PAMI) (2015) 1, 2
- [11] Dosovitskiy, A., Beyer, L., Kolesnikov, A., Weissenborn, D., Zhai, X., Unterthiner, T., Dehghani, M., Minderer, M., Heigold, G., Gelly, S., et al.: An image is worth 16x16 words: Transformers for image recognition at scale. In: Proceedings of the International Conference on Learning Representations (ICLR) (2021) 1, 2, 4, 7, 9
- [12] d'Ascoli, S., Touvron, H., Leavitt, M.L., Morcos, A.S., Biroli, G., Sagun, L.: Convit: Improving vision transformers with soft convolutional inductive biases. In: International Conference on Machine Learning (ICML) (2021) 2
- [13] Ehrlich, M., Davis, L., Lim, S.N., Shrivastava, A.: Quantization guided jpeg artifact correction. In: Proceedings of the European Conference on Computer Vision (ECCV) (2020) 12, 13
- [14] Feichtenhofer, C., Fan, H., Malik, J., He, K.: Slowfast networks for video recognition. In: Proceedings of the IEEE International Conference on Computer Vision (ICCV) (2019) 3, 5
- [15] Feichtenhofer, C., Pinz, A., Wildes, R.: Spatiotemporal residual networks for video action recognition. In: Advances in Neural Information Processing Systems (NeurIPS) (2016) 3

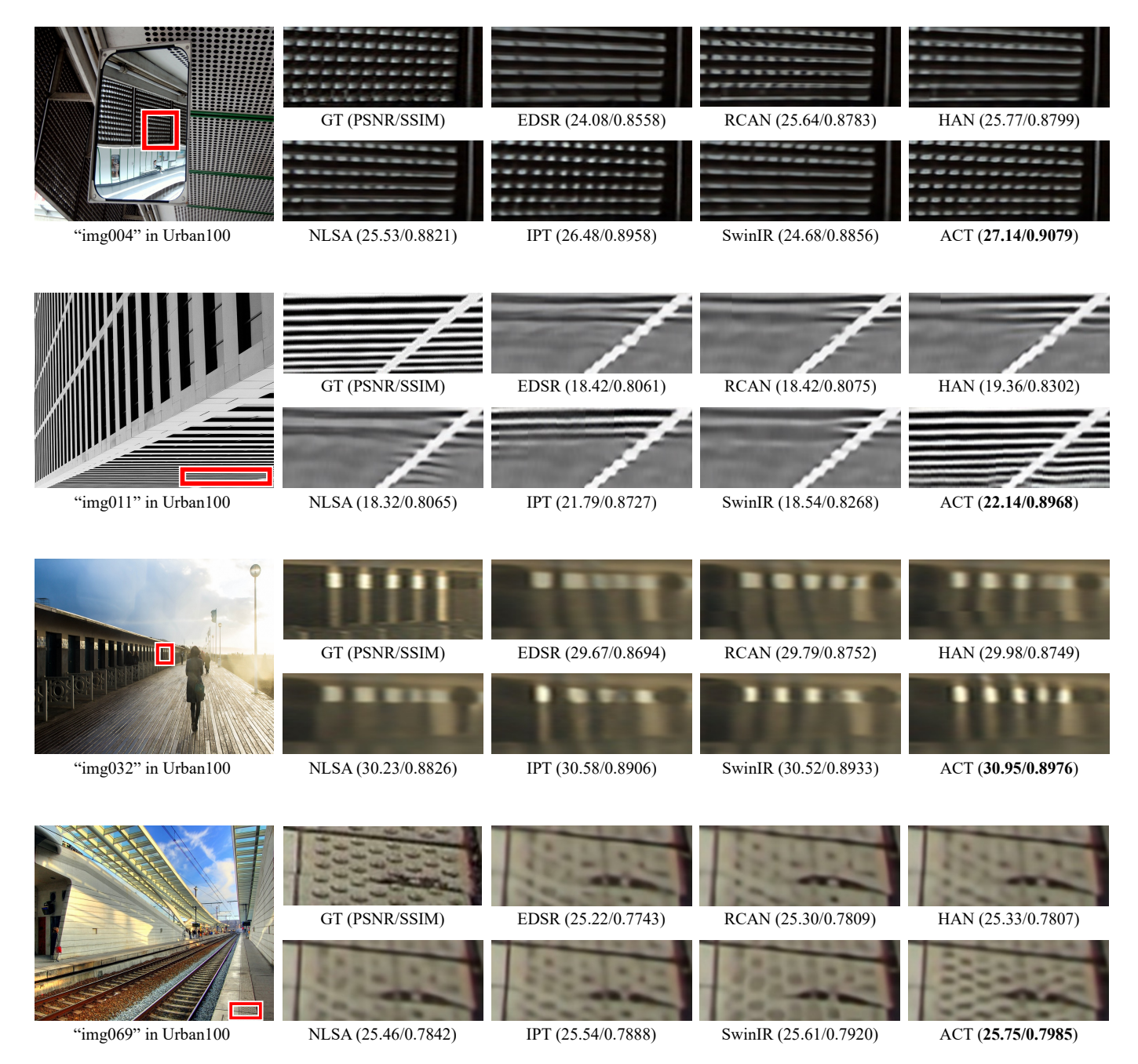


Fig. 11: Visual comparison of the proposed method with various methods for ×4 SR task.

- [16] Feichtenhofer, C., Pinz, A., Wildes, R.P.: Spatiotemporal multiplier networks for video action recognition. In: Proceedings of the IEEE Conference on Computer Vision and Pattern Recognition (CVPR) (2017) 3
- [17] Freeman, W.T., Jones, T.R., Pasztor, E.C.: Example-based super-resolution. IEEE Computer Graphics and Applications (2002) 1
- [18] Glasner, D., Bagon, S., Irani, M.: Super-resolution from a single image. In: Proceedings of the IEEE International Conference on Computer Vision (ICCV) (2009) 1
- [19] Guo, J., Han, K., Wu, H., Xu, C., Tang, Y., Xu, C., Wang, Y.: Cmt: Convolutional neural networks meet vision transformers. arXiv preprint arXiv:2107.06263 (2021) 2
- [20] Guo, Y., Chen, J., Wang, J., Chen, Q., Cao, J., Deng, Z., Xu, Y., Tan, M.: Closed-loop matters: Dual regression networks for single image super-resolution. In: Proceedings of the IEEE Conference on Computer Vision and Pattern Recognition (CVPR) (2020) 2, 3
- [21] He, K., Zhang, X., Ren, S., Sun, J.: Deep residual learning for image recognition. In: Proceedings of the IEEE Conference on Computer Vision and Pattern Recognition (CVPR) (2016) 2, 6
- [22] Hendrycks, D., Gimpel, K.: Gaussian error linear units (gelus). arXiv preprint arXiv:1606.08415 (2016) 4
- [23] Huang, J.B., Singh, A., Ahuja, N.: Single image super-resolution from transformed self-exemplars. In: Proceedings of the IEEE Conference on Computer Vision and Pattern Recognition (CVPR) (2015) 1, 6, 7, 9

- [24] Hui, Z., Wang, X., Gao, X.: Fast and accurate single image super-resolution via information distillation network. In: Proceedings of the IEEE Conference on Computer Vision and Pattern Recognition (CVPR) (2018) 8
- [25] Isobe, T., Jia, X., Gu, S., Li, S., Wang, S., Tian, Q.: Video super-resolution with recurrent structure-detail network. In: Proceedings of the European Conference on Computer Vision (ECCV) (2020) 3
- [26] Jiang, J., Zhang, K., Timofte, R.: Towards flexible blind jpeg artifacts removal. In: Proceedings of the IEEE International Conference on Computer Vision (ICCV) (2021) 12, 13
- [27] Jin, Z., Iqbal, M.Z., Bobkov, D., Zou, W., Li, X., Steinbach, E.: A flexible deep cnn framework for image restoration. IEEE Transactions on Multimedia (TMM) (2019) 3
- [28] Kim, J., Kwon Lee, J., Mu Lee, K.: Accurate image super-resolution using very deep convolutional networks. In: Proceedings of the IEEE Conference on Computer Vision and Pattern Recognition (CVPR) (2016) 1, 2
- [29] Kingma, D.P., Ba, J.: Adam: A method for stochastic optimization. In: Proceedings of the International Conference on Learning Representations (ICLR) (2015) 6
- [30] Ledig, C., Theis, L., Huszár, F., Caballero, J., Cunningham, A., Acosta, A., Aitken, A., Tejani, A., Totz, J., Wang, Z., et al.: Photorealistic single image super-resolution using a generative adversarial network. In: Proceedings of the IEEE Conference on Computer Vision and Pattern Recognition (CVPR) (2017) 1
- [31] Li, Y., Zhang, K., Cao, J., Timofte, R., Van Gool, L.: Localvit: Bringing locality to vision transformers. arXiv preprint arXiv:2104.05707 (2021) 2
- [32] Liang, J., Cao, J., Sun, G., Zhang, K., Van Gool, L., Timofte, R.: Swinir: Image restoration using swin transformer. In: Proceedings of the IEEE International Conference on Computer Vision Workshops(ICCVW) (2021) 1, 2, 6, 8, 9, 10, 12, 13
- [33] Lim, B., Son, S., Kim, H., Nah, S., Mu Lee, K.: Enhanced deep residual networks for single image super-resolution. In: Proceedings of the IEEE Conference on Computer Vision and Pattern Recognition Workshops (CVPRW) (2017) 1, 2, 3, 6, 8, 9, 10, 13
- [34] Liu, D., Wen, B., Fan, Y., Loy, C.C., Huang, T.S.: Non-local recurrent network for image restoration. In: Advances in Neural Information Processing Systems (NeurIPS) (2018) 1, 2
- [35] Liu, Z., Lin, Y., Cao, Y., Hu, H., Wei, Y., Zhang, Z., Lin, S., Guo, B.: Swin transformer: Hierarchical vision transformer using shifted windows. In: Proceedings of the IEEE International Conference on Computer Vision (ICCV) (2021) 2, 9
- [36] Lu, Z., Liu, H., Li, J., Zhang, L.: Efficient transformer for single image super-resolution. arXiv preprint arXiv:2108.11084 (2021) 7
- [37] Martin, D., Fowlkes, C., Tal, D., Malik, J.: A database of human segmented natural images and its application to evaluating segmentation algorithms and measuring ecological statistics. In: Proceedings of the IEEE International Conference on Computer Vision (ICCV) (2001) 6, 7, 9
- [38] Martin, D., Fowlkes, C., Tal, D., Malik, J.: A database of human segmented natural images and its application to evaluating segmentation algorithms and measuring ecological statistics. In: Proceedings of the IEEE International Conference on Computer Vision (ICCV) (2001) 13
- [39] Matsui, Y., Ito, K., Aramaki, Y., Fujimoto, A., Ogawa, T., Yamasaki, T., Aizawa, K.: Sketch-based manga retrieval using manga109 dataset. Multimedia Tools and Applications (2017) 6, 7, 9
- [40] Mei, Y., Fan, Y., Zhou, Y.: Image super-resolution with non-local sparse attention. In: Proceedings of the IEEE Conference on Computer Vision and Pattern Recognition (CVPR) (2021) 1, 2, 8, 9, 10, 13
- [41] Mei, Y., Fan, Y., Zhou, Y., Huang, L., Huang, T.S., Shi, H.: Image super-resolution with cross-scale non-local attention and exhaustive self-exemplars mining. In: Proceedings of the IEEE Conference on Computer Vision and Pattern Recognition (CVPR) (2020) 2, 5
- [42] Niu, B., Wen, W., Ren, W., Zhang, X., Yang, L., Wang, S., Zhang, K., Cao, X., Shen, H.: Single image super-resolution via a holistic attention network. In: Proceedings of the European Conference on Computer Vision (ECCV) (2020) 1, 2, 3, 6, 8, 9, 13
- [43] Park, S., Yoo, J., Cho, D., Kim, J., Kim, T.H.: Fast adaptation to super-resolution networks via meta-learning. In: Proceedings of the European Conference on Computer Vision (ECCV) (2020) 1, 5
- [44] Ranftl, R., Bochkovskiy, A., Koltun, V.: Vision transformers for dense prediction. In: Proceedings of the IEEE International Conference on Computer Vision (ICCV) (2021) 1, 2
- [45] Rao, Y., Zhao, W., Liu, B., Lu, J., Zhou, J., Hsieh, C.J.: Dynamicvit: Efficient vision transformers with dynamic token sparsification. Advances in Neural Information Processing Systems (NeurIPS) (2021) 10
- [46] Rawzor: Image compression benchmark. 13
- [47] Roh, B., Shin, J., Shin, W., Kim, S.: Sparse detr: Efficient end-to-end object detection with learnable sparsity. arXiv preprint arXiv:2111.14330 (2021) 10
- [48] Sheikh, H.: Live image quality assessment database release 2. http://live.ece.utexas.edu/research/quality (2005) 13
- [49] Shi, W., Caballero, J., Huszár, F., Totz, J., Aitken, A.P., Bishop, R., Rueckert, D., Wang, Z.: Real-time single image and video super-resolution using an efficient sub-pixel convolutional neural network. In: Proceedings of the IEEE Conference on Computer Vision and Pattern Recognition (CVPR) (2016) 6, 13
- [50] Shocher, A., Cohen, N., Irani, M.: "zero-shot" super-resolution using deep internal learning. In: Proceedings of the IEEE Conference on Computer Vision and Pattern Recognition (CVPR) (2018) 1, 5
- [51] Simonyan, K., Zisserman, A.: Two-stream convolutional networks for action recognition in videos. In: Advances in Neural Information Processing Systems (NeurIPS) (2014) 3
- [52] Sun, J., Xu, Z., Shum, H.Y.: Image super-resolution using gradient profile prior. In: Proceedings of the IEEE Conference on Computer Vision and Pattern Recognition (CVPR) (2008) 1
- [53] Touvron, H., Cord, M., Douze, M., Massa, F., Sablayrolles, A., Jégou, H.: Training data-efficient image transformers & distillation through attention. In: International Conference on Machine Learning (ICML) (2021) 1
- [54] Vaswani, A., Shazeer, N., Parmar, N., Uszkoreit, J., Jones, L., Gomez, A.N., Kaiser, Ł., Polosukhin, I.: Attention is all you need. In: Advances in Neural Information Processing Systems (NeurIPS) (2017) 1, 2, 4, 5
- [55] Wang, S., Li, B.Z., Khabsa, M., Fang, H., Ma, H.: Linformer: Self-attention with linear complexity. arXiv preprint arXiv:2006.04768 (2020) 10

- [56] Wang, W., Xie, E., Li, X., Fan, D.P., Song, K., Liang, D., Lu, T., Luo, P., Shao, L.: Pyramid vision transformer: A versatile backbone for dense prediction without convolutions. In: Proceedings of the IEEE International Conference on Computer Vision (ICCV) (2021) 2
- [57] Wang, X., Yu, K., Wu, S., Gu, J., Liu, Y., Dong, C., Qiao, Y., Change Loy, C.: Esrgan: Enhanced super-resolution generative adversarial networks. In: Proceedings of the European Conference on Computer Vision (ECCV) (2018) 1
- [58] Wang, Z., Cun, X., Bao, J., Liu, J.: Uformer: A general u-shaped transformer for image restoration. arXiv preprint arXiv:2106.03106 (2021) 1, 2, 13
- [59] Wu, H., Xiao, B., Codella, N., Liu, M., Dai, X., Yuan, L., Zhang, L.: Cvt: Introducing convolutions to vision transformers. arXiv preprint arXiv:2103.15808 (2021) 2
- [60] Yang, J., Wright, J., Huang, T., Ma, Y.: Image super-resolution as sparse representation of raw image patches. In: Proceedings of the IEEE Conference on Computer Vision and Pattern Recognition (CVPR) (2008) 1
- [61] Yuan, L., Chen, Y., Wang, T., Yu, W., Shi, Y., Jiang, Z., Tay, F.E., Feng, J., Yan, S.: Tokens-to-token vit: Training vision transformers from scratch on imagenet. In: Proceedings of the IEEE International Conference on Computer Vision (ICCV) (2021) 1, 4, 12
- [62] Yuan, Y., Fu, R., Huang, L., Lin, W., Zhang, C., Chen, X., Wang, J.: Hrformer: High-resolution transformer for dense prediction. In: Advances in Neural Information Processing Systems (NeurIPS) (2021) 1
- [63] Zeyde, R., Elad, M., Protter, M.: On single image scale-up using sparse-representations. In: International conference on curves and surfaces (2010) 6, 7, 9
- [64] Zhang, Y., Li, K., Li, K., Wang, L., Zhong, B., Fu, Y.: Image super-resolution using very deep residual channel attention networks. In: Proceedings of the European Conference on Computer Vision (ECCV) (2018) 1, 2, 3, 6, 8, 9, 10, 13
- [65] Zhang, Y., Li, K., Li, K., Zhong, B., Fu, Y.: Residual non-local attention networks for image restoration. In: Proceedings of the International Conference on Learning Representations (ICLR) (2019) 1, 2, 8, 9
- [66] Zhou, S., Zhang, J., Zuo, W., Loy, C.C.: Cross-scale internal graph neural network for image super-resolution. In: Advances in Neural Information Processing Systems (NeurIPS) (2020) 2, 8, 9
- [67] Zhu, X., Su, W., Lu, Li, B., Wang, X., Dai, J.: Deformable detr: Deformable transformers for end-to-end object detection. In: Proceedings of the International Conference on Learning Representations (ICLR) (2021) 1, 2
- [68] Zontak, M., Irani, M.: Internal statistics of a single natural image. In: Proceedings of the IEEE Conference on Computer Vision and Pattern Recognition (CVPR) (2011) 1, 2, 8